Biomaterials Science

ROYAL SOCIETY OF CHEMISTRY

PAPER

View Article Online
View Journal | View Issue

Cite this: *Biomater. Sci.*, 2020, **8**, 3611

A novel poly-ε-lysine based implant, Proliferate®, for promotion of CNS repair following spinal cord injury†

Sara Hosseinzadeh,[a] Susan L. Lindsay,[a] Andrew G. Gallagher,[b] Donald A. Wellings,[b] Mathis O. Riehle,[c] John S. Riddell[d] and Susan C. Barnett *[a]

The limited regenerative capacity of the CNS poses formidable challenges to the repair of spinal cord injury (SCI). Two key barriers to repair are (i) the physical gap left by the injury, and (ii) the inhibitory milieu surrounding the injury, the glial scar. Biomaterial implantation into the injury site can fill the cavity, provide a substrate for cell migration, and potentially attenuate the glial scar. We investigated the biological viability of a biocompatible and biodegradable poly-ε-lysine based biomaterial, Proliferate®, in low and high cross-linked forms and when coated with IKVAV peptide, for SCI implantation. We demonstrate altered astrocyte morphology and nestin expression on Proliferate® compared to conventional glass cell coverslips suggesting a less reactive phenotype. Moreover Proliferate® supported myelination *in vitro*, with myelination observed sooner on IKVAV-coated constructs compared with uncoated Proliferate®, and delayed overall compared with maintenance on glass coverslips. For *in vivo* implantation, parallel-aligned channels were fabricated into Proliferate® to provide cell guidance cues. Extensive vascularisation and cellular infiltration were observed in constructs implanted *in vivo*, along with an astrocyte border and microglial response. Axonal ingrowth was observed at the construct border and inside implants in intact channels. We conclude that Proliferate® is a promising biomaterial for implantation following SCI.

Received 20th January 2020,
Accepted 2nd June 2020

DOI: 10.1039/d0bm00097c

rsc.li/biomaterials-science

1. Introduction

Mechanical damage to the spinal cord in traumatic spinal cord injury (SCI) typically induces haemorrhage, blood-spinal cord barrier (BSCB) breakdown, oedema, axonal disruption and demyelination at the injury site.[1] Over time, the injury progresses to secondary and chronic phases commonly comprising cystic cavitation, axonal dieback, demyelination and the formation of a perilesional glial scar.[1,2] Several strategies have been proposed as promising treatments for SCI ranging from cell transplantation to biomaterial implantation.[2] Peripheral nerve grafts implanted into the injured spinal cord have long been known to promote central nervous system (CNS) regeneration by providing a supportive substratum for guided axonal growth.[3–8] However, allogenic peripheral nerve transplantation necessitates long term immunosuppression and autologous transplantation requires further, often non-recoverable, surgery at a secondary site, thereby compounding the existing risk of surgical complications.[9] Biocompatible materials can circumvent this unnecessary harm, providing a substrate for regeneration, a delivery vessel for cell and pharmaceutical therapies,[10–13] and a bridge across cystic cavities formed in intermediate stages of SCI.[14–16]

There is evidence for progressive neurodegeneration and spinal cord atrophy years after SCI,[17] with cavity expansion and continuing die-back of axonal tracts. In pre-clinical studies, cell transplantation reduces injury area as SCI progresses to chronic stages, a finding primarily limited to acute and subacute injury phase transplantations.[18,19] This demonstrates the neuroprotective potential of cell transplantation and consequent physical reconstruction of the injury site. However, cell transplantation in human SCI poses a number of challenges, including generation of cells at numbers high enough to fill large injury cavities and long-term localisation of transplanted cells to the lesion site. By incorporating cells with biomaterials prior to transplantation, cells can be more accurately localised to the lesion site than by injection alone

[a]*Institute of Infection, Immunity and Inflammation, Sir Graeme Davies Building, 120 University Place, University of Glasgow, Glasgow G12 8TA, UK. E-mail: Susan.Barnett@Glasgow.ac.uk; Tel: 44 (0)141 330 8409*
[b]*SpheriTech Ltd, The Heath Business & Technical Park, Runcorn, Cheshire, WA7 4QX, UK*
[c]*Centre for Cell Engineering, Joseph Black Building, University of Glasgow, Glasgow G12 8QQ, UK*
[d]*Institute of Neuroscience and Psychology, West Medical Building, University of Glasgow, Glasgow, G12 8QQ, UK*

†Electronic supplementary information (ESI) available: Fig. S1–S3. See DOI: 10.1039/d0bm00097c

and can be transplanted at lower densities, with the material acting as a substitute ECM to fill the cavity.[10] Several materials, both natural and synthetic, have thus far been investigated for this purpose. The mammalian extracellular matrix (ECM) is an obvious source of natural biomaterials for regeneration, due to its existing cell-supportive role. Indeed, several ECM components have been investigated for SCI implantation, including collagen, fibrin, hyaluronic acid and laminin.[10,12,20–24] Synthetic polymers, however, are often favoured over natural materials for mass reproducibility.[10,12] These polymers can be enriched by incorporation of functional ECM peptides. The most extensively investigated examples of these in CNS repair are Arg-Gly-Asp (RGD), the cell adhesive region of ECM proteins such as laminin and fibronectin,[20–24] and Ile-Lys-Val-Ala-Val [IKVAV], a functional peptide of laminin.[23–27] In particular, IKVAV has been shown to promote neuronal plasticity and improved functional outcomes following rodent SCI.[28,29]

Proliferate®, a polymer based on cross-linked poly-ε-lysine [pεK], is a macroporous, biocompatible and biodegradable material with tuneable porosity. It is composed of two naturally occurring components, pεK and a di-carboxylic acid (*e.g.* decanedioic acid, tridecanedioic acid), breaks down upon decomposition into natural, non-toxic components, and is reproducible on a mass scale. It is a soft, flexible material interspersed with macropores that allow for waste and nutrient exchange, and can bind other bioactive compounds at carboxyl and amine moieties. These included amphotericin B and penicillin G to provide a drug eluting capacity to advanced corneal bandage lenses and addition of the cell binding peptide H-Gly-Gly-Arg-Gly-Asp-Gly-Gly-OH (RGD) as well as fragments of larger proteins such as collagen and fibronectin to promote binding and expansion of corneal endothelial cells *in vitro*.[30–32]

Here we report that Proliferate®, both in original form and when modified by coating in IKVAV, is also a promising candidate for SCI implantation, meeting several criteria for biomaterials in this field including support of CNS cells, integration with CNS tissue and propensity for incorporation of therapeutic compounds.

2. Experimental

2.1. Proliferate® synthesis

Reagents and scaffolds were provided by SpheriTech Ltd (Runcorn, Cheshire, UK). Proliferate® was synthesised from pεK (Zhengzhou Bainafo Bioengineering Co. Ltd, Zhengzhou, China) and cross-linked to 95% (excess amine functional groups) or 105% (excess carboxyl functional groups) with a mix of decanedioic (Sigma Aldrich, Dorset, UK) and tridecanedioic acids (Shanghai Worldyang Chemical Co. Ltd, Shanghai, China) and a polymer density of 0.055 g ml^{-1} using *N*-hydroxysuccinimide (NHS, CarboSynth Ltd, Berkshire, UK) and 1-ethyl-3-(3-dimethylaminopropyl) carbodiimide (EDCI, CarboSynth Ltd, Berkshire, UK).

A pεK (40.9 g, 0.238 mol free amine) monomer stock solution was first prepared in dH_2O (200 ml) and adjusted to pH 7.1. A separate bis-carboxylic acid cross-linker stock solution was also made, composed of tridecanedioic acid (BA; 24.4 g, 0.2 mol of carboxylic acid function), decanedioic acid (SA; 2.24 g, 0.2 mol of carboxylic acid function) and *N*-methylmorpholine (NMM; 25.6 ml, 0.233 mol) in dH_2O (200 ml). A separate stock solution of 5% (w/v) tween 80 (VWR International Ltd, Lutterworth, UK) was also prepared. All stock solutions were filtered separately to 0.45 μm with a nylon + GMF syringe filter (Crawford Scientific Ltd, Strathaven, Scotland).

To make carboxyl-functional Proliferate® (P–C, 105% cross-linking, 50 ml), pεK monomer solution (10 ml) was combined with bis-carboxylic acid cross-linker solution (11.3 ml) and topped up with dH_2O (25 ml). Separately, EDCI (6 g, 31.3 mmol) and NHS (0.69 g, 6 mmol) were dissolved in dH_2O (25 ml) and filter-sterilised before mixing with the pεK/bis-carboxylic acid solution (50 ml total volume). The solution was mixed and immediately poured into 10 × 10 cm^2 Petri dishes (5 ml per dish). The polymer was covered and incubated overnight at 25 °C. The sheets were then washed 1 × 10 min H_2O, 3 × 30 min 0.25 M NaOH, 3 × 30 min 0.25 M HCl, and 3 × 30 min H_2O. Polymer sheets were frozen (approx. −35 °C) on an Edwards Super Modulyo freeze dryer shelf (Edwards Ltd, West Sussex, UK), the vacuum was then applied and they were lyophilised overnight with the shelf reaching a final temperature of 27 °C following an incremental increase. Amine-functional (P–N, 95% cross-linking, 50 ml) constructs were made using the same protocol but with different reagent volumes (10.5 ml pεK stock solution, 10.75 ml bis-carboxylic acid stock solution, 0.66 g NHS, 5.72 g EDCI).

The nonapeptide H-Gly-Gly-Ile-Lys-Val-Ala-Val-Gly-Gly-OH was prepared by solid phase synthesis and purified by reversed phase HPLC. This peptide containing the laminin binding sequence -Ile-Lys-Val-Ala-Val- (IKVAV) was coupled covalently to previously prepared P–C constructs prior to freeze-drying with 0.25 M EDCI and NHS, as follows. A 1 cm length of the CNS conduit (300 mg) with a carboxylic acid capacity of 0.035 mmol was pre-activated with 1-ethyl-3-(3-dimethylaminopropyl)carbodiimide (1.91 g, 10 mmol) and *N*-hydroxy succinimide (1.44 g, 12.5 mmol) in water (50 cm^3) for 1 h. The pre-activated CNS conduit was then washed with water (2 × 50 cm^3) and the nonapeptide (72 mg, 0.07 mmol) pre-dissolved in water (50 cm^3) was added. The coupling reaction was allowed to proceed overnight. The nonapeptide coupled conduit was washed with water (2 × 50 cm^3), sodium hydroxide solution (0.1 mol dm^{-3}, 50 cm^3), water (2 × 50 cm^3), hydrochloric acid solution (0.1 mol dm^{-3}, 50 cm^3) and water (2 × 50 cm^3). The water was drained off and the sample freeze dried to yield 325 mg of nonapeptide coupled CNS conduit. The amount of peptide coupled (25 mg) was determined gravimetrically.

Two glycine amino acids either side of the IKVAV have been shown to minimise aggregation (Spheritech unpublished observations). The initial loading of IKVAV to the polymer was

monitored *via* HPLC. At different time-points in the polymerisation process, the supernatant was collected and run on the HPLC to monitor the amount of peptide left in the supernatant. The decreasing amount in the supernatant indicated the binding of peptide to the polymer. In order to confirm the presence of the IKVAV peptide on the carboxyl scaffold, one dry carboxyl scaffold sample and one dry IKVAV carboxyl scaffold sample were sent for amino acid analysis (Severn Biotech Ltd, Kidderminster). The samples were hydrolysed and separated, and the amino acids were detected and quantified compared to their predicted values of 1 isoleucine, 1 lysine, 2 valine and 1 alanine. The detection of lysine was excluded because of the large amounts of lysine found in the poly(ε-lysine) polymer. The IKVAV carboxyl was compared to the carboxyl scaffold in relation to their amino acid content. The coupling protocol is well established and fully validated[33] therefore the only quality control carried out was gravimetric analysis of the construct prior and post coupling of the peptide. IKVAV coupling to biomaterial scaffolds is a well-established procedure.[34–36]

To make 24-well plate construct inserts, the dry sheets were cut to 0.64 cm^2 with a size 5 borer. Blank (no membrane attached) 24-well cell culture inserts (SABEU GmbH & Co. KG, Northeim, Germany) were adhered to the construct using a dissolution/reprecipitation technique. The blank inserts were aligned on top of the 0.64 cm^2 constructs before adding toluene dropwise (40 μl). The insert was then inverted and left to dry for 1 h. To make tubular constructs for implantation, a 1 ml serological pipette (3 mm in diameter) was secured vertically using a clamp and 300 soluble polyvinyl alcohol fibres (100 μm diameter, soluble at 90 °C), were inserted vertically through the pipette, and secured at each end with cable ties. P–C was prepared as described and poured into a 1 ml syringe upon combination with the cross-linker solution. The syringe was inverted and attached to the serological pipette, and the polymer solution was syringed upwards to fill the pipette. The construct was left to set for 5 h, following which the pipette and polymer within were cut into 40 mm segments using a pipe cutter and scalpel respectively. The pipette sections containing the construct were placed in a water bath at 100 °C for 8 h to dissolve the fibres whilst retaining morphology. The constructs were removed from the pipette sections, washed further with water at 100 °C (×5) and freeze-dried as described above (see schematic in ESI Fig. 1†). The constructs were examined *via* SEM for wash efficiency.

Prior to cell seeding or implantation, constructs were sterilised in 70% ethanol for >2 h and incubated in cell culture medium overnight. For *in vivo* implantation, constructs were washed and stored in endotoxin-free PBS following sterilisation, prior to surgery.

2.2. Mechanical characterisation

Mechanical properties of Proliferate® was measured using a Linkam TST350 tensile tester (Linkam Scientific Instruments Ltd, Tadworth, England). Stress (σ), strain (ε) and elastic modulus (E) were determined for each hydrated sample. Samples were cut to a dog bone shaped piece using a bore to provide a 15 mm test length between the clamps of the Linkam stage. The width and thickness of each sample was measured with an Absolute Digimatic caliper (Mitutoyo Ltd, Andover, England) and the readings recorded. The sample was then mounted in the Linkam tensile tester and secured in place with the provided clamps. The software was run and each sample was elongated until breakage point. A 20 N load cell was used for all mechanical analysis with a strain rate of 100 μm s^{-1}. Results were recorded and analysed using the supplied Linksys32 software.

2.3. Ethical considerations

All experimental procedures were approved by the Ethical Review Panel of the University of Glasgow and performed in accordance with the UK Animals (Scientific Procedures) Act 1986 using ARRIVE guidelines. Animals were kept under appropriate light and temperature conditions, with food and water available *ad libitum*.

2.4. Cell culture

Primary glial and neural cells isolated from Sprague-Dawley (SD) rats (Charles River) were maintained in a humidified incubator at 37 °C with 7% atmospheric CO_2. Astrocytes were cultured from postnatal day 1 (P1) rat neurospheres according to standard methods previously described.[37] Briefly, neurospheres were obtained from striatum dissections, cultured for 7–10 days *in vitro* (DIV), resuspended and cultured in astrocyte culture media (10% foetal bovine serum (FBS) in low glucose Dulbecco's modified Eagle's medium (DMEM), both ThermoFisher). Astrocyte cultures were fed twice weekly and reached confluency at 5–7 DIV. Myelinating cultures were generated from embryonic day 15 (E15) rats and seeded onto confluent neurosphere-derived astrocyte monolayers as previously described.[37] E15 spinal cord preparations were initially cultured in high glucose DMEM (ThermoFisher) containing 10 ng ml^{-1} biotin (Sigma-Aldrich), 50 nM N1 medium supplement (Sigma-Aldrich), 50 nM hydrocortisone (Sigma-Aldrich) and 0.5 mg ml^{-1} bovine insulin (ThermoFisher) for 12 days. Insulin was removed from culture media for the remaining culture period (up to 40 DIV). Myelinating cultures were fed three times weekly. All culture media was supplemented with 0.5 μg ml^{-1} gentamycin.

Glia cells or myelinating cultures were plated onto Proliferate® constructs as described above or onto poly-L-lysine (PLL, Sigma-Aldrich) coated 13 mm glass coverslips (VWR) in 24-well plates. 20 ml PLL solution (13.3 μg ml^{-1} in dH_2O) was used per 96 coverslips. 500 μl culture media was added to wells containing suspended construct inserts prior to cell seeding, and a 50–100 μl cell suspension was added and incubated for 1 h. Wells were then topped up with a further 500 μl media. Cultures were fed by removing 500 μl media surrounding the insert and replacing with 500 μl media directly onto the insert.

2.5. Implantation *in vivo*

Contusion procedures were carried out on adult male Sprague-Dawley rats as previously described,[19] with modifications to

impact force and injury level as follows. Animals were anaesthetised with isoflurane and a laminectomy was performed to expose the spinal cord at the C6 level. A midline impact with a force of 175 kdyn was administered using an Infinite Horizon impactor (Precision Systems Instrumentation). The contusion site was marked by a 10-0 Ethicon suture in the dura, the wound was closed and animals recovered in heated cabinets. Implantation of Proliferate® constructs was performed 3 weeks after contusion, allowing sufficient time for cavity formation. The injury site was re-opened and the contusion cavity identified by the marking suture. An incision was made in the dura at this site, revealing the fluid-filled cavity. Cavity fluid was aspirated with care using a blunted 23 G needle. The tubular construct containing parallel-aligned channels was cut to the size of the injury cavity and implanted in alignment with the cord. The material is compliant (sponge like) in consistency and so could be eased through this slit-like opening, displacing the edges of the dorsal columns to fill the cavity. Once this is done, the spared tissue of the dorsal columns spring back over the top of the biomaterial so that there is minimal scarring or contact of the biomaterial with the dura. Adherence problems and the potential to disrupt the integrity of the tissue containing the injury site and implants were therefore minimal due to the injury model and implant approach adopted. The dura was closed again over the injury, with a marking suture placed at the implantation site. In all procedures, animals received pre- and post-operative analgesics (buprenorphine, 0.05 mg kg^{-1} and carprofen, 5 mg kg^{--1}, s.c.). Saline (3–5 ml) and enrofloxacin (5 mg kg^{-1}) were given s.c. for 3 and 7 days respectively following surgery. If motor impairment was detected following recovery, animals were excluded from the study. Animal numbers and experimental design is summarised in Fig. 1. Twenty-eight animals were contused, of which 6 were excluded due to motor impairment or inadequate recovery. No significant difference was observed in animal weights at contusion and implantation procedures (Fig. 4C and D), or in actual force and displacement achieved (Fig. 4E–H). Subsequently, 7 animals received P–C implants, of which 1 was excluded, and 9 received P–IK implants, of which 2 were excluded. Injury histology was assessed at short term (7 weeks) and long-term (6 months) time points.

2.6. Scanning electron microscopy [SEM]

Proliferate® constructs were mounted onto specimen stubs (Agar Scientific) using conductive carbon tape and silver paint was applied to construct edges. Stubs were coated with 10–20 nm gold palladium using a Quorum Q150 T high vacuum coater. To visualise cell monolayers grown on the construct, samples were prepared prior to coating using the following protocol. Cultures were fixed for 1 h at RT using 1.5% glutaraldehyde in 0.1 M sodium cacodylate buffer. Samples were then washed in 0.1 M sodium cacodylate buffer, before being incubated in 1% osmium tetroxide in sodium cacodylate buffer for 1 h. Samples were rinsed once more in buffer before washing 3 × 10 min in dH_2O, and incubating in 0.5% uranyl acetate in dH_2O for 1 h, protected from light. Samples were

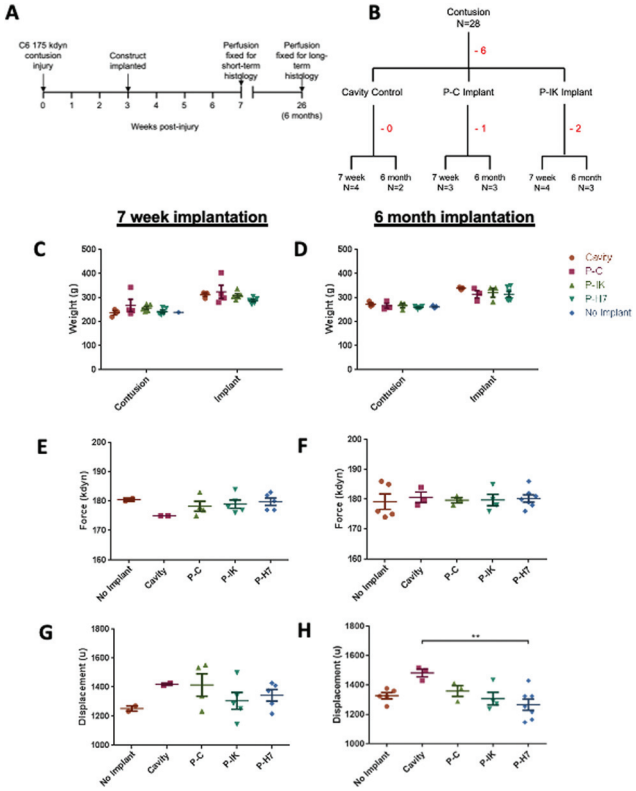

Fig. 1 *In vivo* experimental design and injury parameters. [A] Summary of experimental timeline. [B] Summary of total animals implanted. Body weights were similarly distributed with no significant difference across experimental groups [one-way ANOVA] both for animals perfused after 7 weeks [C] and 6 months [D]. Injury force [E, F] and displacement [G, H] were similarly distributed across experimental groups [one-way ANOVA] for animals implanted for both 7 weeks [E, G] and 6 months [F, H]. Error bars = mean ± SEM.

then progressively dehydrated in the following ethanol concentrations: 30% (10 min), 50% (10 min), 70% (10 min), 90% (10 min), absolute (4 × 5 min) and dried absolute (4 × 5 min). The dried absolute ethanol solution contained a 3A molecular sieve (Sigma-Aldrich) to remove moisture. A final drying step was then carried out in hexamethyldisilazane (HDMS) before mounting onto specimen stubs and coating as described. Samples were visualised on a JEOL6400 scanning electron microscope running at 10 kV, and images were captured using the Olympus Scandium Software.

2.7. Western blot

Cells were lysed using CellLytic M containing protease inhibitor cocktail (Sigma-Aldrich), and protein concentrations were determined using a BCA protein assay (ThermoFisher) according to manufacturer's instructions. Samples were run on tris-acetate gels and transferred using the iBlot™ gel transfer device (Invitrogen). Membranes were blocked in 5% milk in 0.2% Triton X-100 in TBS (TBS-T) for 1 h before being incubated with anti-GFAP (1 : 100 000, DAKO) for 2 h, and with anti-nestin (1 : 1000, Merck Millipore) overnight at 4 °C. Blots were washed in TBS-T and incubated 1 h

with secondary antibody (ECL rabbit IgG, ECL mouse IgG, GE Healthcare). The protein loading control used was GAPDH (1 : 1000, Abcam). Band intensities were quantified using Image-J and normalised to GAPDH.

2.8. Immunocytochemistry

Cultures were fixed in 4% paraformaldehyde (PFA, in PBS at PH 7.4) and permeabilised with 0.1% Triton X-100. Primary antibodies (GFAP anti-rabbit 1 : 1000, DAKO; nestin anti-mouse IgG1 1 : 500, SMI-31 anti-mouse IgG1 1 : 1000, both Merck Millipore; β-III-tubulin anti-rabbit 1 : 1000, Abcam; PLP 1 : 00, hybridoma), were diluted in blocking buffer (0.2% gelatin (Sigma-Aldrich) in PBS) and incubated for 1 h at RT. Samples were washed three times in PBS before incubation with fluorescent-conjugated secondary antibodies (AlexaFluor 1 : 1000, ThermoFisher) for 45 min at RT. Coverslips were washed and mounted in an aqueous mounting medium (25 mg ml^{-1}, 4-diazabicyclo[2.2.2]octane (DABCO), Sigma-Aldrich) containing Hoechst 33342 nuclear dye (NucBlue™, ThermoFisher). Specimens were imaged using an Olympus BX51 fluorescent microscope.

2.9. Histology

Animals were deeply anaesthetised with intraperitoneal sodium pentobarbital (200 mg ml^{-1} Euthatal, Vericore) and transcardially perfused with mammalian Ringer solution containing 0.1% lidocaine. Animals were subsequently perfused with 4% PFA in 0.1 M PBS (1 L PFA per animal). Spinal cord segments containing the implant were dissected, leaving approximately 10 mm tissue on either side of the injury site, and submerged in cryoprotective post-fixation solution (30% sucrose in 4% PFA) overnight. Tissue blocks were then submerged in 30% sucrose in PBS for 24 h, or until the tissue was observed to sink. Dura were removed, and cords were cut to 6–9 mm blocks containing the injury site, as determined by injury extent. Blocks were notched dorso-ventrally before being frozen in OCT. Sixty μm sections were cut sagittally using a cryotome at −20 °C and incubated free-floating in 0.3 M PBS.

Sections were incubated in 50% ethanol for 30 min, washed 3× in PBS for 10 min, and incubated in primary antibodies (GFAP 1 : 1000, ThermoFisher; nestin anti-mouse IgG1 1 : 500, Merck Millipore; Laminin anti-rabbit 1 : 500, Sigma-Aldrich; ED-1 anti-mouse IgG1 1 : 500, BioRad; Neurofilament 200 anti-mouse IgG1 1 : 1000, Sigma-Aldrich) for 72 h at 4 °C. Sections were washed a further 3 × 10 min in PBS before incubation with secondary antibodies (AlexaFluor 1 : 1000, ThermoFisher) for 3 h at 4 °C, protected from light. Sections were then washed 3 × 10 min in PBS, mounted on glass slides in aqueous mounting. Sealed slides were stored at −20 °C, protected from light.

All sections were first examined using a Zeiss Axioplan epifluorescence microscope to identify sections with the largest cavity size, and to inspect immunolabeling. Representative sections selected were considered the most medial injury sections. Selected illustrative sections were scanned with a Zeiss LSM 710 confocal system using X20 and X63 objective lenses. Laser excitation wavelengths used for scanning were 405, 488, 561 and 633 nm. Tissue sections were scanned as tiled composites of multiple fields at low (×20) and high (×63) magnification. Sections were scanned throughout the stained tissue to accumulate a series of optical sections at 2–5 μm z separation. Stacked images were projected into 2D maximum intensity projections using Zeiss Zen software (Zeiss, Germany).

2.10. Quantification of cavity extent

Sagittal sections from each injury block were viewed under an epifluorescence microscope and rostral and caudal limits of the injury identified by the construct-tissue border signified by construct autofluorescence, or in control sections from cavity rims. Sections containing the most extensive sites (at least 3 per block) were selected for confocal imaging and the maximal injury length and height were measured using ZEN lite 2010 software (Zeiss). Injury site width was quantified by counting the number of sections containing the injury and multiplying by section thickness (60 μm).

2.11. Statistical analysis

All statistical analysis was carried out using GraphPad Prism software. A one-way ANOVA, with Dunnett's or Tukey's *post hoc* tests where appropriate, was used for null hypothesis statistical testing, where a $p < 0.05$ was considered statistically significant. For *in vitro* analysis, N indicates biological replicates incorporating a minimum of 3 technical replicates. For *in vivo* analysis, N indicates separate animals.

3. Results

3.1. Proliferate® macro- and micro-structure

Mechanical and surface properties of Proliferate® in carboxyl-functional form (P–C, highly cross-linked) are shown in Fig. 2. For the present investigations, Proliferate® was synthesised in for culture in two ways: (i) suspended in 24-well cell culture inserts for 3D culture (Fig. 2A and C) and (ii) in tubular form containing parallel-aligned cell guidance channels (Fig. 2B and D). Microscopically, Proliferate® presents a heterogenic beaded 3D topography. This heterogeneity creates natural surface peaks and troughs to give rise to a heterogeneously porous topography (Fig. 2E–G), tuneable by the degree of cross-linking. Tensile testing revealed Proliferate®'s Young's modulus as 0.0128 kPa (Fig. 2H).

3.2. Astrocytes alter morphology and reactivity status on Proliferate® *in vitro*

Astrocytic interactions with Proliferate® were investigated by culturing neurosphere-derived primary neonatal rat astrocytes on suspended Proliferate® cell culture inserts. These types of astrocytes were used as they are a feature of the myelinating cultures used to study CNS cell differentiation (section 3.3). Cells were cultured on Proliferate® in carboxyl-functional (P–C, high cross-linkage), amine-functional (P–N, low cross-linkage) and IKVAV-coated (P–IK) forms. Astrocytes adopted a more fibrous, branched morphology on all forms of

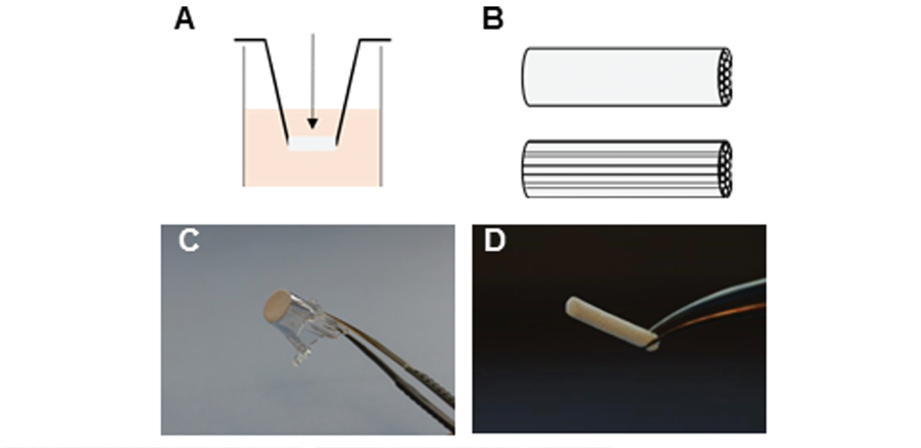

H

Ultimate tensile stress (kPa)	Failure strain	Young's Modulus (kPa)
0.014	1.11	0.0128

Fig. 2 Proliferate® is a porous, structurally versatile and biocompatible polymer. Proliferate® was suspended in 24-well plate inserts for *in vitro* cell culture [A, C, arrow indicates direction of cell seeding] and fabricated in tubular form with parallel-running channels for *in vivo* implantation [B, D]. SEM images show the porous heterogeneity of Proliferate® microstructure [E, scale bar = 100 μm], its characteristic 3D beaded topography in high power [F, scale bar = 5 μm], and parallel-channels incorporated within Proliferate® in tubular form [G, scale bar = 100 μm]. [H] Mean mechanical properties of Proliferate® as obtained by tensile testing [*N* = 6]. Data is shown for carboxyl-functional Proliferate® [P–C] only.

Proliferate® compared to those grown on PLL-coated coverslips as visualised both by GFAP and nestin labelling (Fig. 3A) and scanning electron microscopy (SEM, Fig. 3B). To investigate astrocyte reactivity on Proliferate®, GFAP and nestin expression in these cultures were quantified by western blot as markers of astrocyte reactivity. GFAP upregulation is a well-established marker for reactivity *in vitro* and *in vivo*, but not a definitive one due to high expression in quiescence and heterogeneous expression across CNS tissue and in culture.[38] Nestin was therefore used as a supplementary reactivity marker, as GFAP-nestin co-expression is an indicator of astrocyte reactivity *in vivo*[39] and is characteristic of these cultures *in vitro*.[40] No significant difference was observed in GFAP expression between astrocyte cultures on Proliferate® and controls, however nestin was significantly lower on P–C and P–N than on PLL-glass (Fig. 3C). Nestin expression also appeared reduced on P–IK, although this difference was not significant.

3.3. Neuron survival and neurite extension and myelination on Proliferate® *in vitro*

To investigate the potential of Proliferate® for guiding axonal growth in the spinal cord, embryonic spinal cord suspensions were cultured on astrocyte monolayers (myelinating cultures, MCs) to examine the ability for cells to develop neurites and for myelination. Neurites were present at both 33 DIV (Fig. 4A) and 40 DIV (Fig. 4B). Myelination, as indicated by proteolipid protein (PLP, green) immunolabelling, was delayed on constructs compared with PLL-glass. Myelination, as seen by the formation of sheaths, is ordinarily observed on MCs at 28 DIV,[37] however this is not clearly observed until 33 DIV on P–IK, and 40 DIV on P–C and P–N (Fig. 4A and B), showing that constructs can support myelination but that this is delayed compared with cultures on PLL-glass. Axonal density appears lower on constructs compared with PLL-glass, though this may be due to axonal dispersal through the greater surface area in Proliferate® constructs.

3.4. Proliferate® prevents long-term cavity expansion *in vivo*

Proliferate® was implanted into adult rat contusion spinal cord injuries *in vivo*. As no difference was observed *in vitro* in cell viability, growth and myelination between P–C and P–N, only P–C was implanted as the non-coated construct control, alongside the IKVAV-coated P–IK. GFAP labelling revealed a distinct astrocytic border surrounding injury cavities and con-

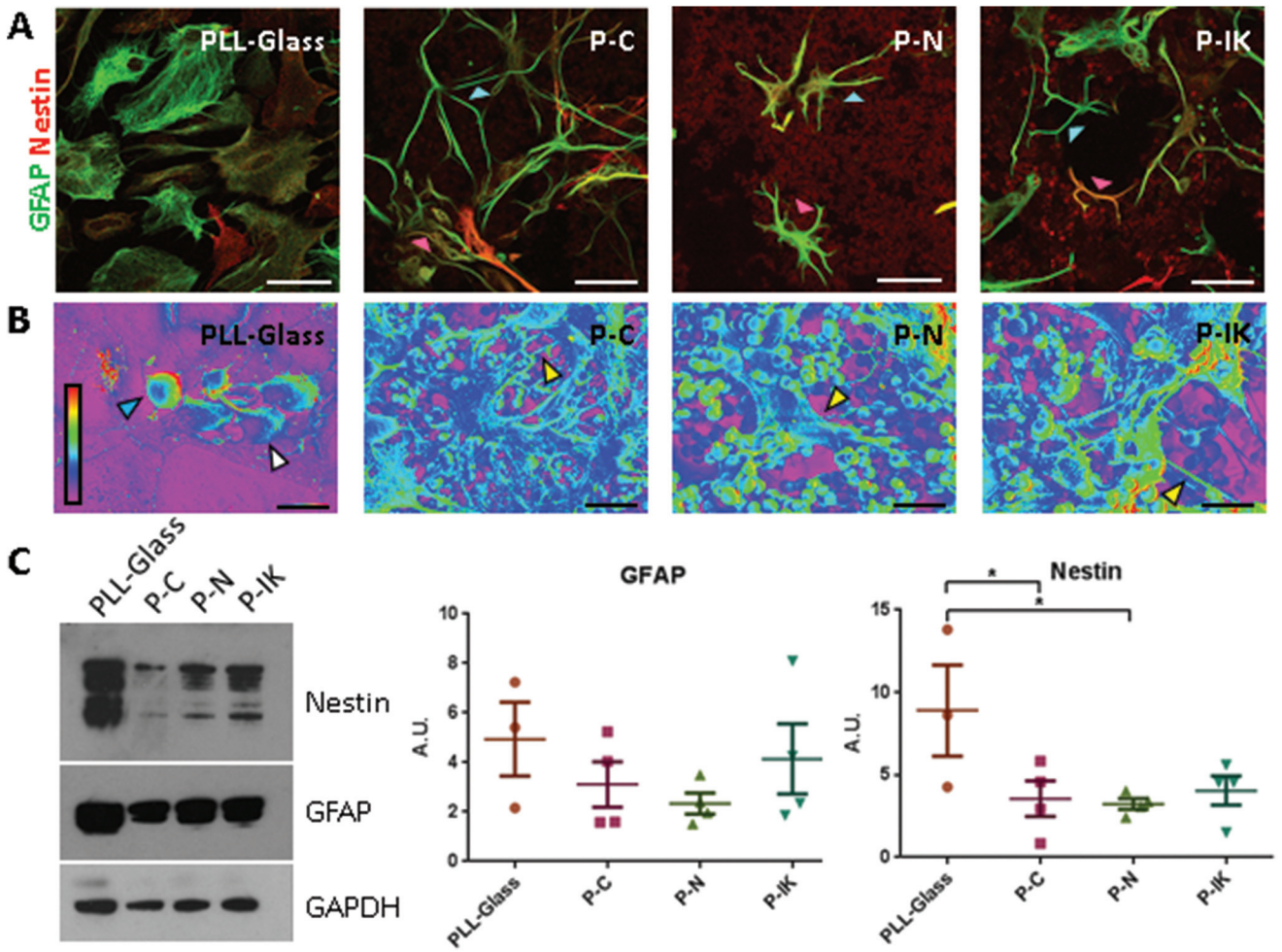

Fig. 3 Astrocytes adopt fibrous morphology and reduce nestin expression on Proliferate® compared with PLL-glass. [A] Neurosphere-derived astrocytes cultured in serum-containing media on P–C, P–N and P–IK compared with PLL-glass, labelled with anti-GFAP [green] and anti-nestin [red]. Astrocytes adopt a fibrous, branched morphology on all forms of the construct compared with flat, expansive morphologies on PLL-glass. Astrocytes extend processes both over the construct surface [pink arrows] and across pores [A, blue arrows]. Construct surfaces are visualised by non-specific anti-nestin labelling. Scale bar = 50 μm. [B] SEM images of neurosphere-derived astrocytes on P–C, P–N and P–IK compared with PLL-glass, at 2000× magnification, illustrating cell-construct interactions. Construct appears mostly pink in colour, and cells blue/green. Some beaded polymer construct segments also appear blue/green but are morphologically distinct from cells. Note that not all the construct surface is covered by the pink area, some of the beads are the same colour as the cells. Astrocytes on PLL-glass extend processes from elevated nuclei [B, white arrow], with undifferentiated neurospheres [B, blue arrow] also sporadically visible. On P–C, P–N and P–IK, astrocyte cell bodies are anchored to the construct surface with fibres outstretched multi-directionally [B, yellow arrows]. Scale bar = 10 μm. [C] GFAP and nestin expression on P–C, P–N and P–IK compared with PLL-glass after 7 DIV in serum-containing culture. Nestin expression is reduced on P–C and P–N compared with PLL-glass, paralleled by non-significant trends towards nestin reduction on P–IK, and GFAP reduction on all construct substrates compared with PLL-glass. Data from protein samples extracted from confluent astrocytes at 7 DIV [one-way ANOVA with Dunnett's *post-hoc* test, $P < 0.05$. Error bars: mean ± SEM. $N = 4$].

struct implants in both implanted and non-implanted injuries (Fig. 5) persistent at both 7 weeks (A–C) and 6 months post-implantation (D–F). At both time points, however, the GFAP cavity-tissue border in non-implanted injuries appears starker than that of implanted injuries, with some astrocytes appearing to enter scaffolds at the construct-tissue border in implanted cavities (highlighted in Fig. 5A–Fii), suggesting that construct-tissue borders are more permissive to astrocyte growth and migration than cavity-tissue borders. GFAP delineation coupled with non-specific staining of Proliferate® by anti-nestin antibody reveals the full extent of cavities and implants (Fig. 5B, C, E and F). Quantification of cavity extent (Fig. 6) reveals no difference in cavity length 7 weeks post-implantation (Fig. 6C) compared with non-implanted control cavities, however significantly lower rostral-caudal cavity extremities (cavity length) in P–C and P–IK are observed in implanted injuries than in non-implanted injuries 6 months post-implantation ($p < 0.05$. Fig. 6F). No significant difference is observed in lateral cavity extremities (cavity width) between implanted and non-implanted sections at either time point. The longitudinal measurement is more significant in this context as there is evidence that contusion cavities continue to

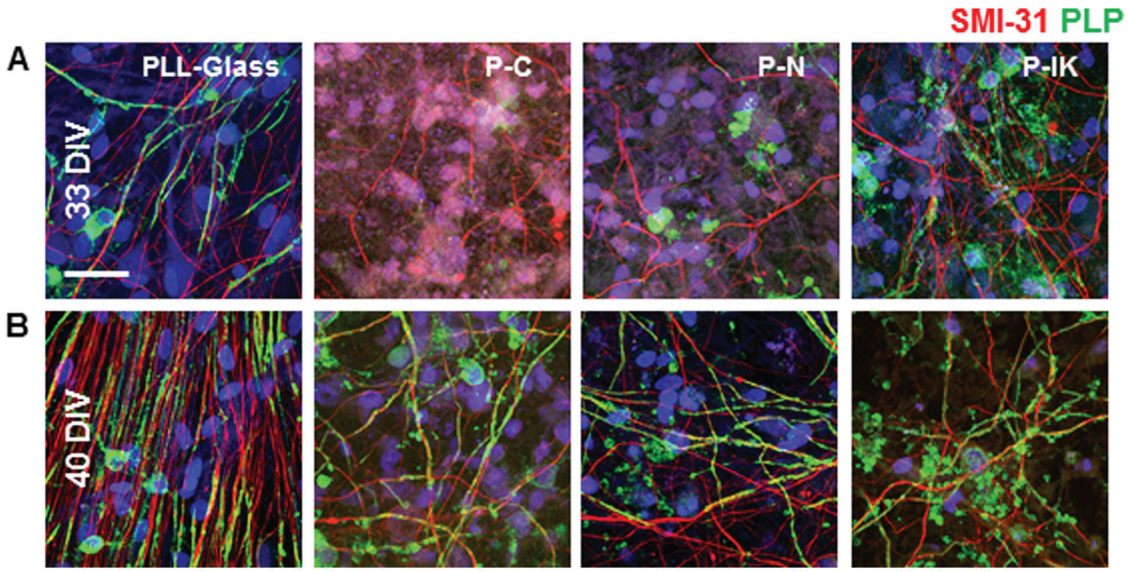

Fig. 4 Neuronal survival and myelination on Proliferate®. Myelinating cultures labelled with anti-SMI31, anti-PLP and Hoechst 33342, at [A] 33 DIV and [B] 40 DIV on P–C, P–N and P–IK compared with PLL-glass. Myelination is delayed on 3D Proliferate® substrates compared with glass. Scale bar = 20 μm.

expand in this plane for up to 6 months after injury whereas changes in width are minimal (J. S. Riddell & M. Hadian, unpublished observations). It is notable that channel integrity does not appear to be maintained in implants, with only few open channels visible on histological examination (highlighted by dashed lines).

3.5. Proliferate® induces extensive vascularisation and cellular influx *in vivo*

Laminin labelling revealed extensive vascularisation throughout construct implants both 7 weeks and 6 months post-implantation (Fig. 7, ESI Fig. 2†). Clear laminin vessels are present throughout P–C and P–IK implanted constructs, abundantly surrounded by nuclei (Fig. 7). Notably, vascularisation and cellular influx occurred throughout constructs both in guidance channels and in construct-dense regions. Non-specific construct labelling by Hoechst 33342 nuclear stain is observed, however nuclei are identifiable by morphology (ESI Fig. 3†).

3.6. Microglial response to Proliferate® *in vivo*

To assess the immunological response to construct implants, microglia and macrophages in injury cavities and construct implants were visualised by anti-ED-1 labelling (green, Fig. 8). Although microglia were present in constructs both centrally and at the construct-tissue border, they accounted for only a small population of Hoechst 33342 stained nuclei within and surrounding constructs at both 7 weeks and 6 months post-implantation (Fig. 8A and B). No clear difference was observed in microglial response between 7 weeks and 6-month time points (see ESI Fig. 2†). In non-implanted injuries, a distinct tissue-cavity border was observed through which microglia and other cells did not cross due to lack of matrix infilling acting as a cell support (Fig. 8C). No clear difference was visible in microglial levels surrounding non-implanted injury cavities and construct-implanted injuries.

3.7. Neurite growth into Proliferate®-implanted lesions

Axonal outgrowth from perilesional zones into construct implants remains limited at both short- and long-term time points, as visualised by neurofilament labelling (Fig. 9). No clear difference was observed in axonal growth into constructs between 7 weeks and 6-month time points. Inside constructs, axons remain sparse at both time points, and are limited to segments of undisrupted guidance channels (Fig. 9A). At the construct tissue border, however, axons appear to grow out from perilesional zones into Proliferate® implants with regularity in segments with intact guidance channels providing spaces for entry (Fig. 9B). Non-implanted injuries maintain a binary axonal border between tissue and injury cavity, with no axonal outgrowth observed (Fig. 8C).

4. Discussion

Previously, we demonstrated *in vitro* the potential of aligned micropatterned ε-polycaprolactone (PCL) as an biomaterial for SCI,[41,42] however due to concerns pertaining to the stiffness disparity between these PCL scaffolds and the spinal cord, our findings had limited potential for *in vivo* application. We found the stiff PCL was hard to position into a lesion and did not appear to integrate well (unpublished observations). Therefore, pεK based Proliferate® scaffolds were selected as an alternative implantable scaffold with material properties more closely comparable to spinal cord tissue. With no preconditioning, the Young's modulus of the adult rat spinal cord has

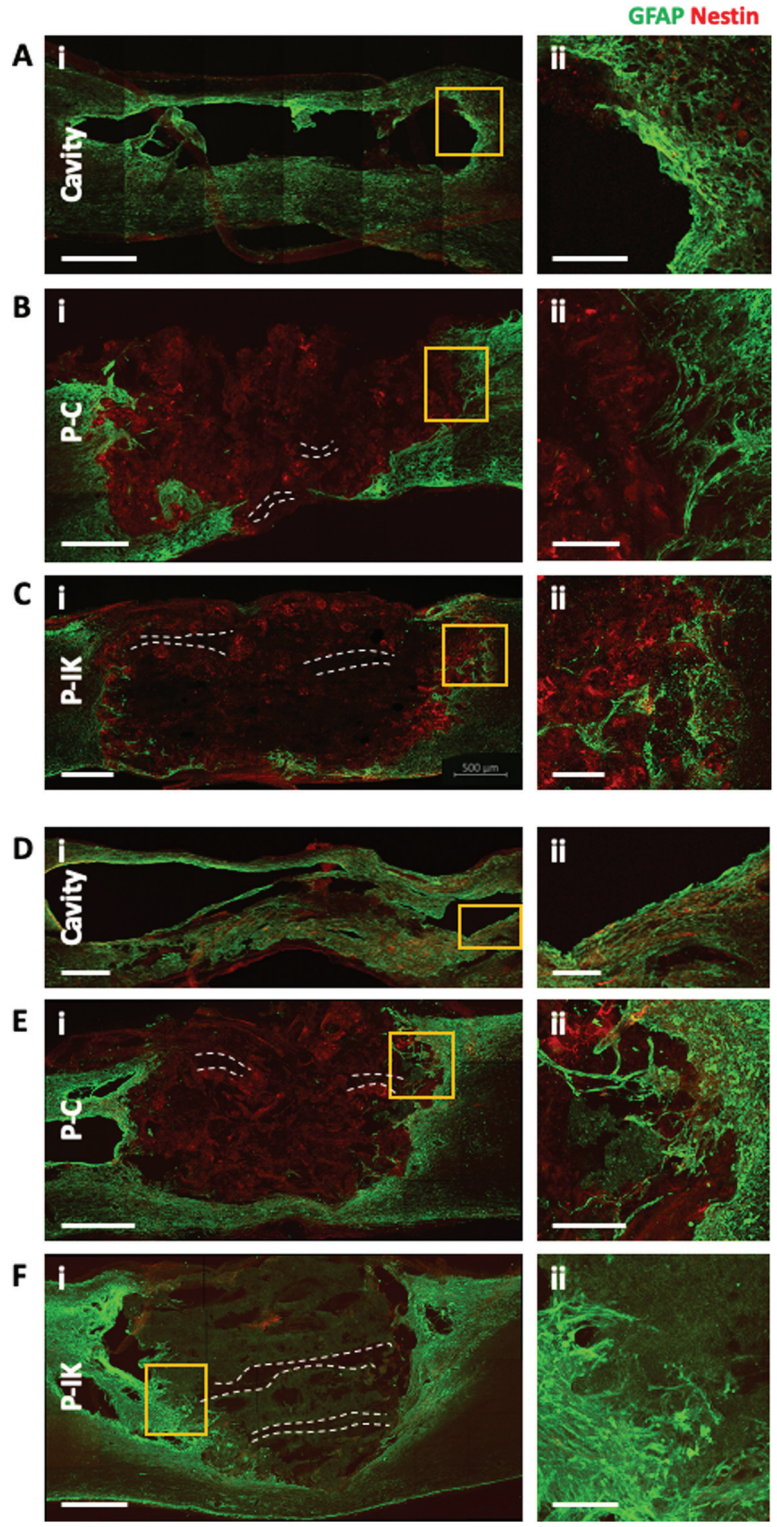

Fig. 5 Anti-GFAP and anti-nestin labelling delineates construct-tissue border and indicates cavity extent. [A] Anti-GFAP [green] labelling reveals distinct construct-tissue astrocytic borders of injury cavities at both 7 weeks [A–C] and 6 months [D–F] post-implantation. GFAP + cells are sparsely seen entering the constructs at both time points [as highlighted in A–F ii]. Non-specific nestin labelling [red] allows construct visualization. Some non-specific weakly fluorescent anti-GFAP construct staining is also observed [notable in F]. Parallel channels fabricated in constructs are largely absent, with channels only sparsely visible [highlighted by dashed lines, notable in F]. Scale bars [i] 500 μm, [ii] 125 μm. Tile-scan confocal images, 20× magnification, 2–5 μm *z*-separation.

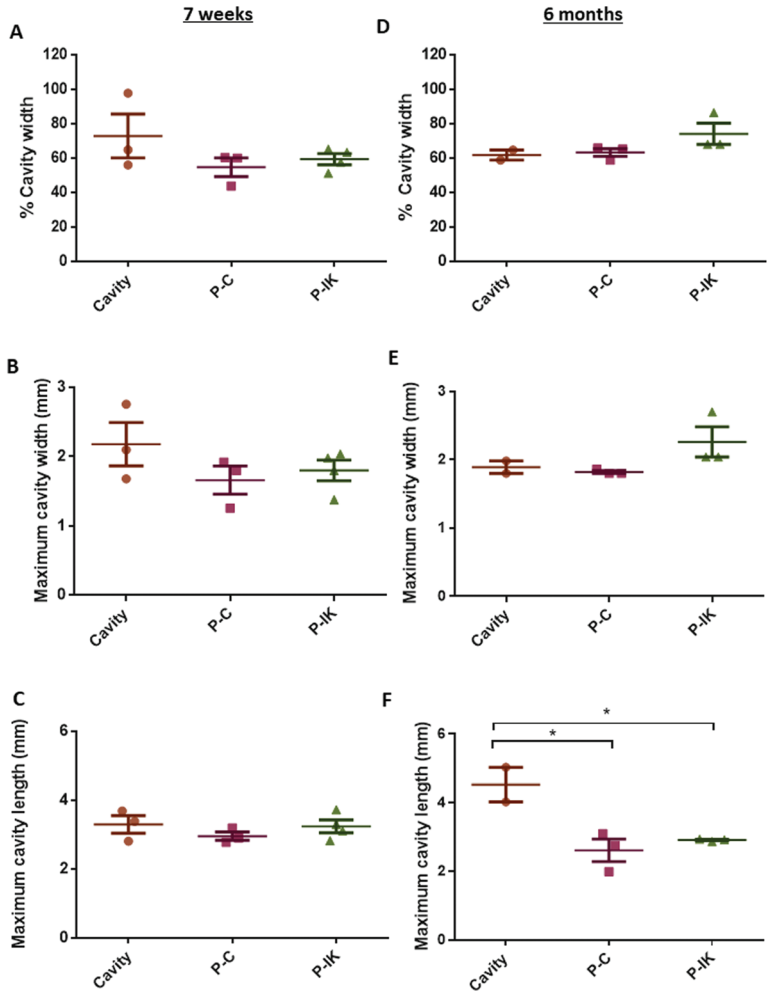

Fig. 6 Proliferate® prevents chronic cavity expansion. The percentage of the total cord width occupied by the injury cavity [A, D] and the maximum cavity width in each injury [B, E] do not differ significantly across experimental groups 7 weeks or 6 months post-implantation [one-way ANOVA]. Maximum cavity length does not differ significantly across experimental groups at 7 weeks post-implantation [C], but is lower in P–C and P–IK-implanted injuries at 6 months post-implantation compared to non-implanted controls [F, one-way ANOVA].

been estimated at 0.15–0.74 kPa.[43] Proliferate® in carboxyl-functional form has a Young's modulus of 0.0128 kPa, comparable closely to these recent findings. We therefore concluded that Proliferate® is mechanically compatible with the rat spinal cord and proceeded to test for corresponding CNS biocompatibility using various neural cell cultures.

Astrocytes play a large role in the glial scar following SCI, and are highly responsive to biomaterial topographies.[41,44] On the three different Proliferate® substrates tested, astrocytes adopted a stellate, ramified morphology distinct from the flat, expansive polygonal morphology observed on flat PLL-glass coverslips. This morphology is typical of astrocytes *in vivo*,[45] therefore suggests that Proliferate® surface topography is comparable to the 3D tissue milieu in which these cells inherently reside. The heterogeneously beaded surface topography of Proliferate® is more reminiscent of 3D spinal cord tissue than flat glass coverslips typically used for cell culture. Consistent with our findings, astrocytes adopt ramified morphologies on a range of other 3D biomaterials, including alginate, collagen type 1, collagen-hyaluronic acid (HA) and collagen-HA-matrigel hydrogels,[46–48] polyurethane nanofibers[49] and hydrophobic tripalmitin.[50] It has been shown that when astrocytes are cultured in 3D hyrogel their morphology resembles perivascular astrocytes, but they also from round, stellate or bipolar shapes within a few days. The latter is induced by aligned microcolumns,[47,51–53] however the branched morphology is considered most representative of *in vivo* phenotypes.[45] Moreover, it has been shown that astrocytes form a reparative phenotype as assessed by reduced GFAP expression and fewer F-/G-actin stress fibres when plated on 3D electrospun bioscaffolds relative to 2D astrocytes.[54] The broad consensus in the field is that for better understanding of astrocytic behaviour, particularly with respect to the characterisation of the spectrum of astrocyte reactivity states, astrocyte culture systems must be optimised to promote representative *in vivo* astrocytic states.[40,55] To this aim, other modifications of the culture

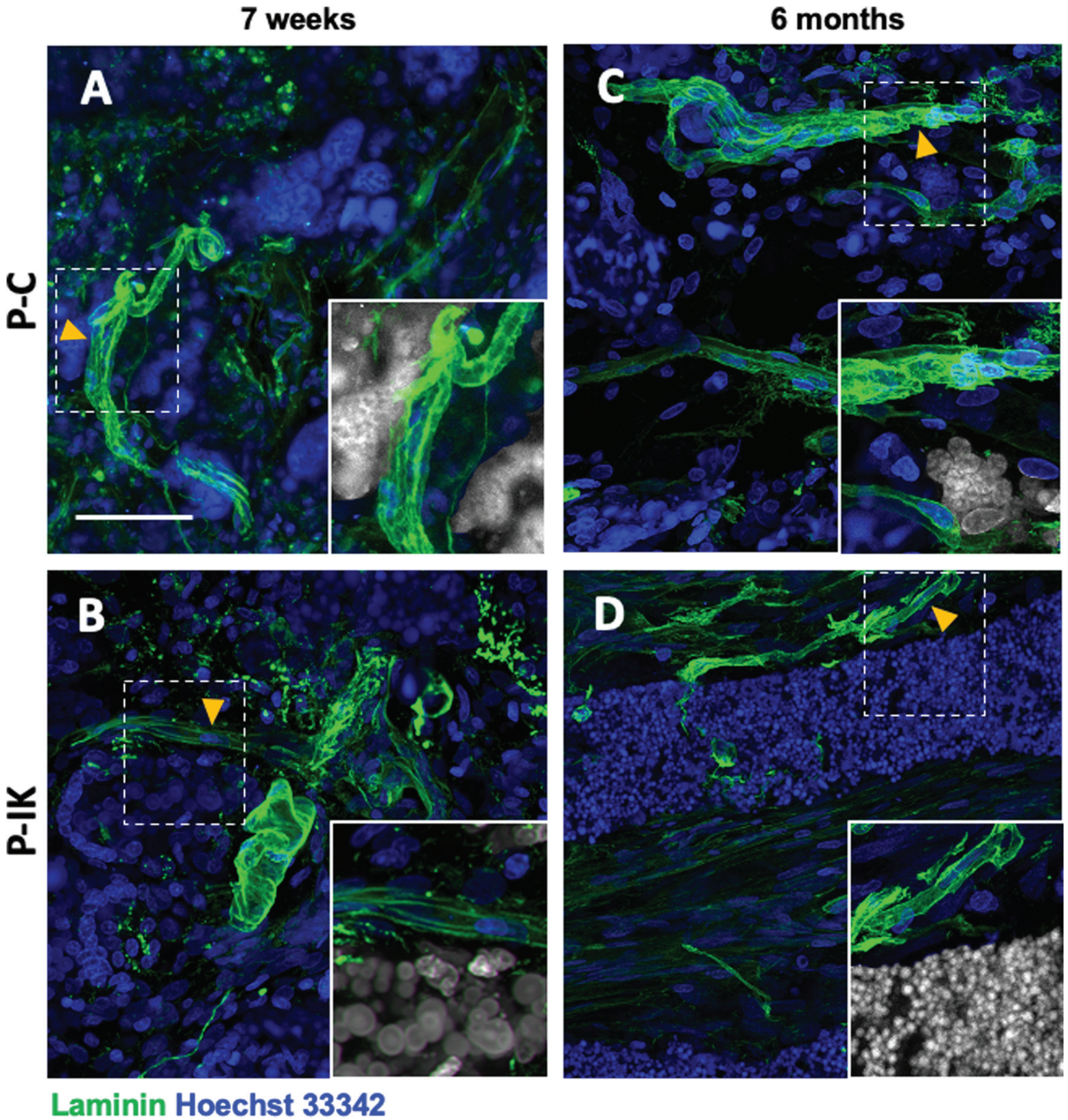

Fig. 7 Extensive vascularisation is observed in construct-implanted injuries. Anti-laminin staining shows tubular blood vessels [highlighted by arrows and insert] present extensively and uniformly throughout P–C [A, C] and P–IK [B, D]-implanted injuries both 7 weeks [A, B] and 6 months [C, D] post-implantation. In highlighted regions (inset), construct is shown in grey. Scale bar = 50 μm. Confocal images, 63× magnification, 2–5 μm *z*-separation.

environment, separate from substrate characteristics, have also been used to promote a ramified morphology. Media modifications, including the removal of serum from culture media, and immunopanning are one example of this, being reported to promote astrocyte phenotypes closer to those seen *in vivo* both morphologically and, in protein and gene expression profiles.[56–58]

No definitive protein markers of astrocyte reactivity have thus far been identified, though increased GFAP expression has long been the accepted hallmark.[55,59] However, GFAP is largely expressed by quiescent astrocytes and astrocytes *in vitro*. Therefore, alongside quantification of GFAP in cultures on Proliferate® and PLL-glass, we also quantified nestin expression as an indicator of reactivity. Nestin is an intermedi-

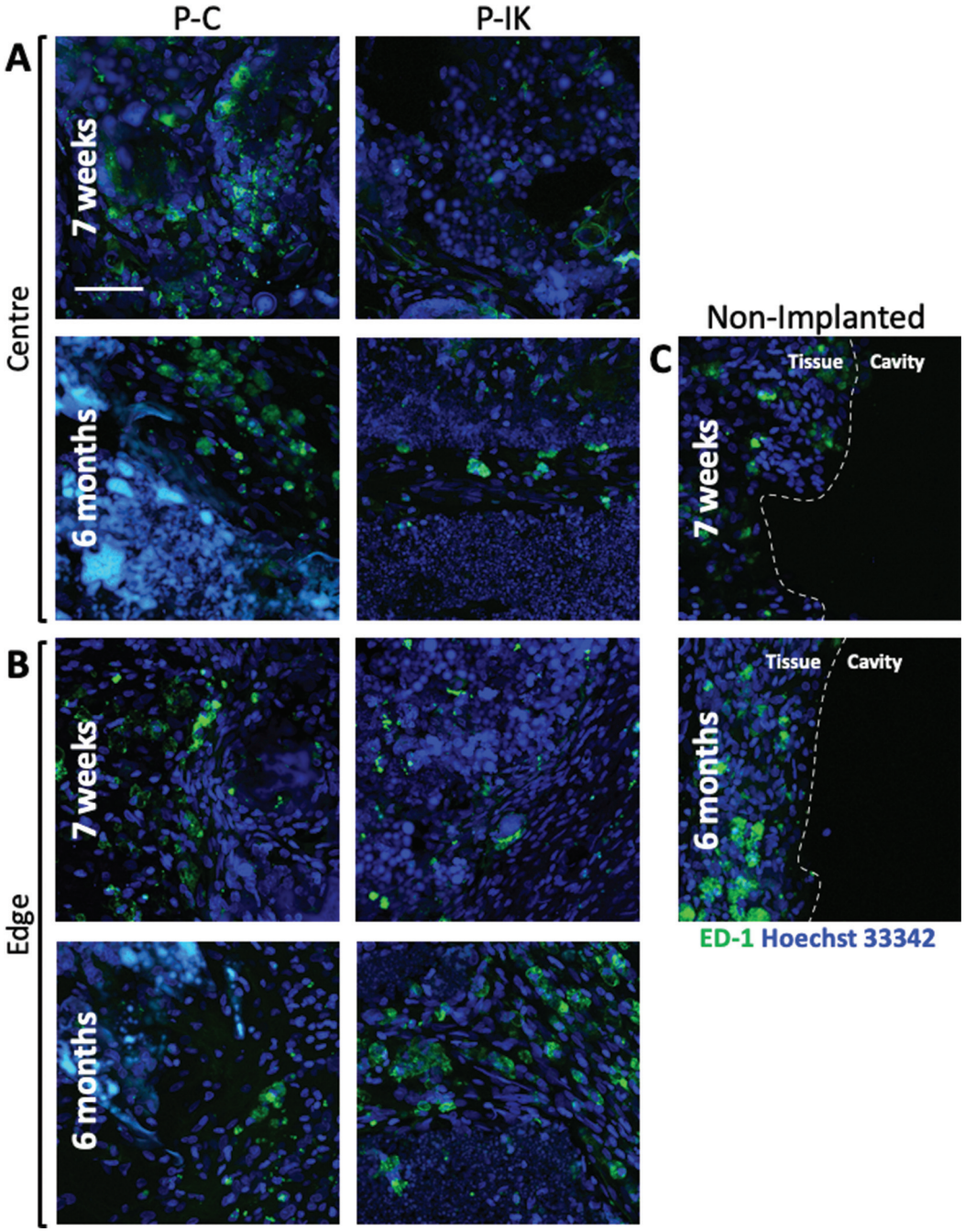

Fig. 8 Microglial response to Proliferate®. Anti-ED1 antibody labelling [green] shows microglia present [A] in the center and [B] at the edges of P–C and P–IK implanted injuries both 7 weeks and 6 months post-implantation. Microglia did not migrate into non-implanted cavities due to a lack of matrix infilling to act as a growth or migration substrate, resulting a clear tissue-cavity border at the lesion edge [C]. Scale bar = 50 μm. Confocal images, 63× magnification, 2–5 μm *z*-separation.

ate filament protein predominantly expressed in neural development,[60,61] and re-expressed by reactive astrocytes.[62,63] Astrocytic nestin expression is common in traditional cell culture conditions, however is absent in non-reactive spinal cord *in vivo*.[39] In traditional astrocyte culture, nestin expression is lower on non-coated Proliferate® (P–C, P–N) than on 2D PLL-glass, indicating an altered astrocyte reactivity state on the construct reminiscent of *in vivo* quiescence. As the astrocyte-mediated glial scar remains one of the greatest barriers to CNS repair, the potential induction of a quiescent-like phenotype by Proliferate® could be viewed positively, however it is important to note that astrocyte reactivity and the glial scar are also implicated in several beneficial functions alongside detrimental ones.[38]

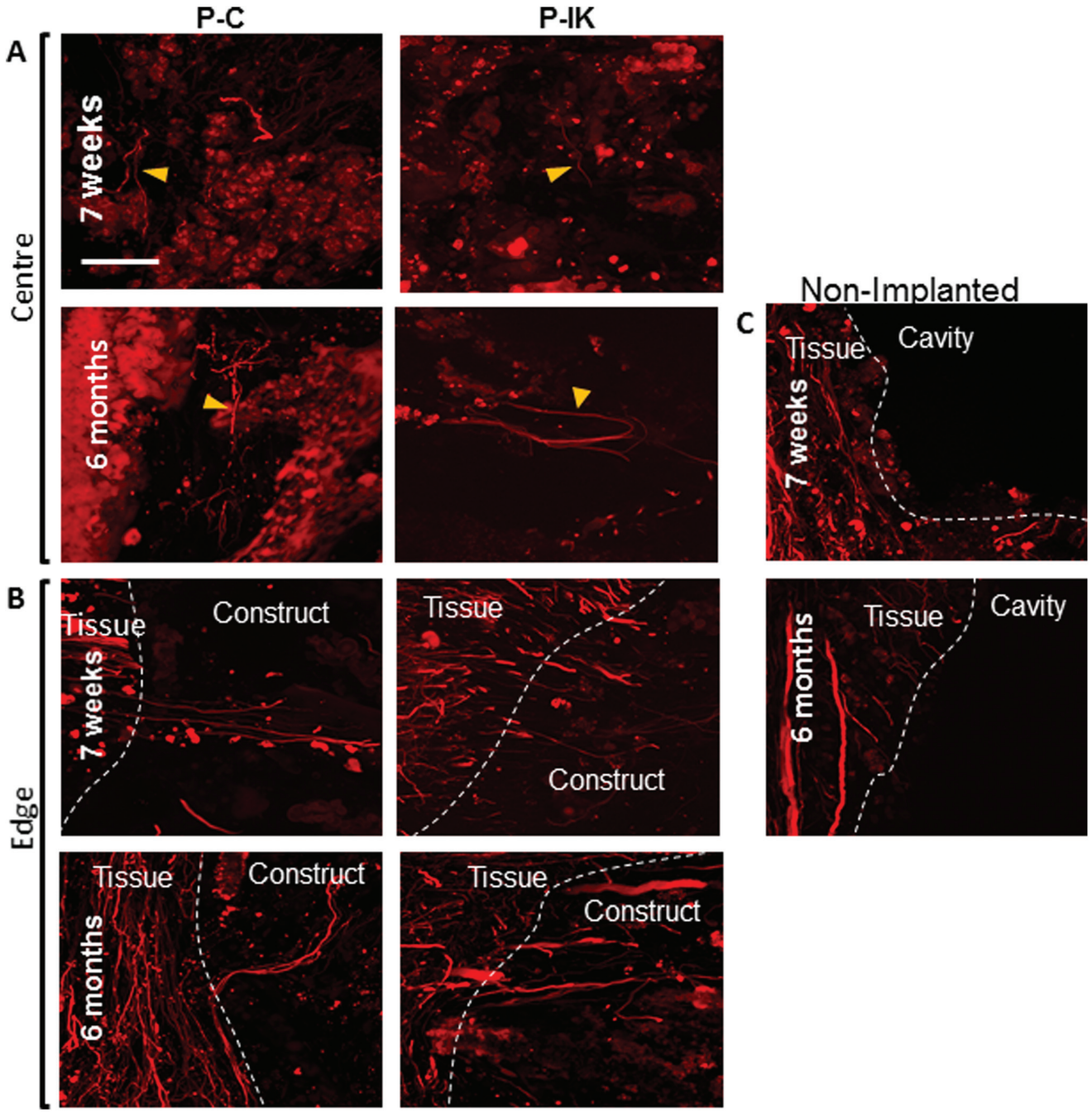

Fig. 9 Neurite outgrowth can be seen within Proliferate®. Anti-neurofilament [red] staining demonstrates axonal outgrowth from perilesional zones into construct implants although limited at both short- and long-term time points. [A] Axons can be detected inside constructs [highlighted by arrows], although remain sparse and are limited to segments of undisrupted guidance channels. [B] At the construct tissue border, axons can be seen to extend from perilesional tissue into Proliferate® implants [tissue-construct border highlighted by dashed lines]. [C] Non-implanted injuries maintain a binary axonal border between tissue and injury cavity, with no axonal outgrowth observed [tissue-cavity border highlighted by lines]. Confocal images, 63× magnification, 2–5 μm *z*-separation.

Neuronal morphological differences are also seen between PLL-glass and Proliferate® substrates. On flat glass surfaces, axons appear to grow largely in parallel outwards from cell body bundles dispersed throughout coverslips.[37] Conversely, on Proliferate® substrates cell bodies appear more evenly dispersed throughout the culture without bundling, and axonal orientation is no longer organised in parallel fashion. Axonal alignment in the spinal cord is important for physiological function, therefore for Proliferate® to be viable as an implantable material, the incorporation of guidance cues into the material may be crucial. Myelination was delayed in these cultures on Proliferate®, continuous with our previous findings

on PCL.[41] This may due to a lack of neurite organisation or a substrate-specific delay in oligodendrocyte maturation, as was postulated in our PCL study. This also may be due to the difference in stiffness between glass and proliferate which can also affect aspects of differentiation.[64] Myelination was, however, observed on P–IK earlier than on P–C and P–N in our study. However the important observations is that all CNS glial cells can interact, differentiate and form myelin sheaths on Proliferate®.

For implantation *in vivo*, Proliferate® was fabricated in tubular form containing parallel channels for more organised guidance. However, upon histological examination 7 weeks/6 months following implantation, channels did not remain intact, with only remnants of the channel organisation visible at both time points. We postulate that due to the soft nature of Proliferate®, channel walls are prone to adhering and/or collapsing upon compression induced by surgical procedures and movement of the spinal column. We believe that by using soluble fibres of larger diameter to fabricate channels, channel integrity may be more consistently maintained. At 6 months following implantation, non-implanted injuries were more extensive, as indicated by higher rostral-caudal cavity lengths, than those implanted with Proliferate®. This indicates stabilisation of the injury by adhesion of constructs to perilesional tissue, preventing excessive tissue dieback. As rostral-caudal cavity lengths were not significantly different in implanted than in non-implanted injuries at 7 weeks post-implantation, it suggests that this dieback is a chronic injury response. A distinct astrocytic border was observed surrounding constructs in both short and long-term implantations, as is expected of typical non-implanted contusion injuries, however the reactivity status of these astrocytes is unclear. The prevalence of quiescent-like astrocytic phenotypes on Proliferate® substrates *in vitro* with low nestin expression could be indicative of a similar phenotype *in vivo*, however due to non-specific construct labelling by the nestin antibody, co-expression of GFAP and nestin could not be accurately quantified by immunohistochemistry. We did note, however, sporadic evidence of visible astrocytic movement from the perilesional zones into constructs in areas of channel integrity at the border with existing gaps for inward cellular movement. Similar astrocytic bordering has been observed surrounding collagen nanofiber implants in C3 rat hemisection injury[65] and T10 rat contusion injuries implanted with poly(lactic-*co*-glycolic acid) (PLGA) and PCL.[66] Astrocytic ingrowth was, however, observed in collagen scaffold implanted T8–10 hemisection[67] and transection[68] injuries, and in poly (*N*-[2-hydroxypropyl]methacrylamide) hydrogel (NeuroGel™) implanted into T6–7 complete cat transections, where glial scar formation was attenuated.[69]

Evidently, several non-astrocytic cells do move into Proliferate® implants, as nuclei that are not associated with either GFAP or nestin are visible extensively throughout constructs at both 7 weeks and 6 months post-implantation, as is extensive vascularisation. The presence of vascular structures across constructs lays the foundations for cell ingrowth. The identity of these cells, however, remains elusive. Microglia are one cell type ordinarily prevalent in SCI, however we found that microglia represent only a minority of cells in construct implants at both time points investigated, appearing in similar quantities both in the centre of constructs and at astrocyte-rich construct borders.

The ultimate goal of construct implantation is to promote neuronal regeneration across the injury site. However, as previously discussed, guidance cues are paramount to organised axonal growth and alignment. Cell guidance channels are one example of such cues,[11] however as previously mentioned, guidance channels incorporated into P–C and P–IK implants did not retain integrity once implanted. Organised axonal extension across injuries were therefore not possible. Congruently, axonal growth into construct implants was observed only in areas where intact channels existed. It was promising, however, that in such regions axons were able, though in small number, to grow into constructs. In these areas, some axons were observed in construct centres as well as edges, particularly in implants maintained to 6 months.

5. Conclusion

The therapeutic value of biomaterial implantation in SCI is multi-faceted. Our findings have shown a novel material, Proliferate®, to possess the necessary material properties for this purpose. We have demonstrated the compatibility of CNS cells with Proliferate® *in vitro* and *in vivo*, showing Proliferate®'s potential both as a solo implant, and as a base upon which other therapeutic compounds can be immobilised for delivery of other bioactive molecules to the injury site, for example molecules affecting the glial scar or facilitation of axonal regeneration. It will then be appropriate to investigate whether these mechanistic actions translate into tangible improvements in functional outcome by carrying out behavioural or electrophysiological assessments.

Author contributions

S. H. carried out all the *in vitro* work and *in vivo* analysis, S. L. L. help with *in vivo* work and analysis. J. S. R. carried out the animal model of spinal cord injury, S. C. B. and M. O. R. supervised the study and obtained funding. AGG and DAW provided the Proliferate® and supervised the biomaterial work. All authors reviewed and commented on the manuscript.

Conflicts of interest

Proliferate®, based polymer is marketed by SpheriTech but there are no financial contribution between the University of Glasgow and SpheriTech. The authors declare that they have no competing interests.

Acknowledgements

This work was supported by the Medical Research Scotland (SH, grant numbers 718-2013-169822-91); the Multiple Sclerosis Society of Great Britain, (SLL grant number 56).

References

1 C. S. Ahuja, *et al.*, Traumatic spinal cord injury, *Nat. Rev. Dis. Primers*, 2017, **3**, 17018.
2 A. P. Tran, P. M. Warren and J. Silver, The biology of regeneration failure and success after spinal cord injury, *Physiol. Rev.*, 2018, **98**(2), 881–917.
3 P. M. Richardson, U. M. McGuinness and A. J. Aguayo, Axons from CNS neurones regenerate into PNS grafts, *Nature*, 1980, **284**(5753), 264.
4 S. David and A. J. Aguayo, Axonal elongation into peripheral nervous system" bridges" after central nervous system injury in adult rats, *Science*, 1981, **214**(4523), 931–933.
5 P. M. Richardson, U. M. McGuinness and A. J. Aguayo, Peripheral nerve autografts to the rat spinal cord: studies with axonal tracing methods, *Brain Res.*, 1982, **237**(1), 147–162.
6 P. M. Richardson, V. M. K. Issa and A. J. Aguayo, Regeneration of long spinal axons in the rat, *J. Neurocytol.*, 1984, **13**(1), 165–182.
7 G. M. Bray, *et al.*, The use of peripheral nerve grafts to enhance neuronal survival, promote growth and permit terminal reconnections in the central nervous system of adult rats, *J. Exp. Biol.*, 1987, **132**(1), 5–19.
8 P. Tabakow, *et al.*, Transplantation of autologous olfactory ensheathing cells in complete human spinal cord injury, *Cell Transplant.*, 2013, **22**(9), 1591–1612.
9 M.-P. Côté, *et al.*, Peripheral nerve grafts support regeneration after spinal cord injury, *Neurotherapeutics*, 2011, **8**(2), 294–303.
10 S. Liu, *et al.*, Biomaterial-supported cell transplantation treatments for spinal cord injury: challenges and perspectives, *Front. Cell. Neurosci.*, 2018, **11**, 430.
11 A. E. Haggerty and M. Oudega, Biomaterials for spinal cord repair, *Neurosci. Bull.*, 2013, **29**(4), 445–459.
12 K. S. Straley, C. W. P. Foo and S. C. Heilshorn, Biomaterial design strategies for the treatment of spinal cord injuries, *J. Neurotrauma*, 2010, **27**(1), 1–19.
13 A. M. Ziemba and R. J. Gilbert, Biomaterials for local, controlled drug delivery to the injured spinal cord, *Front. Pharmacol.*, 2017, **8**, 245.
14 M. D. Norenberg, J. Smith and A. Marcillo, *The pathology of human spinal cord injury: defining the problems*, Mary Ann Liebert, Inc., 2004.
15 C. H. Tator, Update on the pathophysiology and pathology of acute spinal cord injury, *Brain Pathol.*, 1995, **5**(4), 407–413.
16 T. H. Milhorat, *et al.*, Pathological basis of spinal cord cavitation in syringomyelia: analysis of 105 autopsy cases, *J. Neurosurg.*, 1995, **82**(5), 802–812.
17 G. Ziegler, *et al.*, Progressive neurodegeneration following spinal cord injury: implications for clinical trials, *Neurology*, 2018, **90**(14), e1257–e1266.
18 A. Toft, *et al.*, Electrophysiological evidence that olfactory cell transplants improve function after spinal cord injury, *Brain*, 2007, **130**(4), 970–984.
19 S. L. Lindsay, *et al.*, Human olfactory mesenchymal stromal cell transplants promote remyelination and earlier improvement in gait co-ordination after spinal cord injury, *Glia*, 2017, **65**(4), 639–656.
20 S. M. Amr, *et al.*, Bridging defects in chronic spinal cord injury using peripheral nerve grafts combined with a chitosan-laminin scaffold and enhancing regeneration through them by co-transplantation with bone-marrow-derived mesenchymal stem cells: Case series of 14 patients, *J. Spinal Cord Med.*, 2014, **37**(1), 54–71.
21 J. Cao, *et al.*, The use of laminin modified linear ordered collagen scaffolds loaded with laminin-binding ciliary neurotrophic factor for sciatic nerve regeneration in rats, *Biomaterials*, 2011, **32**(16), 3939–3948.
22 S. Hou, *et al.*, The repair of brain lesion by implantation of hyaluronic acid hydrogels modified with laminin, *J. Neurosci. Methods*, 2005, **148**(1), 60–70.
23 S. Woerly, *et al.*, Spinal cord repair with PHPMA hydrogel containing RGD peptides (NeuroGel™), *Biomaterials*, 2001, **22**(10), 1095–1111.
24 A. Hejčl, *et al.*, HPMA-RGD hydrogels seeded with mesenchymal stem cells improve functional outcome in chronic spinal cord injury, *Stem Cells Dev.*, 2010, **19**(10), 1535–1546.
25 V. M. Tysseling-Mattiace, *et al.*, Self-assembling nanofibers inhibit glial scar formation and promote axon elongation after spinal cord injury, *J. Neurosci.*, 2008, **28**(14), 3814–3823.
26 Y. T. Wei, *et al.*, Hyaluronic acid hydrogels with IKVAV peptides for tissue repair and axonal regeneration in an injured rat brain, *Biomed. Mater.*, 2007, **2**(3), S142.
27 J. Park, *et al.*, Nerve regeneration following spinal cord injury using matrix metalloproteinase-sensitive, hyaluronic acid-based biomimetic hydrogel scaffold containing brain-derived neurotrophic factor, *J. Biomed. Mater. Res., Part A*, 2010, **93**(3), 1091–1099.
28 V. M. Tysseling, *et al.*, Self-assembling peptide amphiphile promotes plasticity of serotonergic fibers following spinal cord injury, *J. Neurosci. Res.*, 2010, **88**(14), 3161–3170.
29 S. Kazemi, *et al.*, IKVAV-linked cell membrane-spanning peptide treatment induces neuronal reactivation following spinal cord injury, *Future Sci. OA*, 2015, **1**(4), FSO81.
30 A. G. Gallagher, *et al.*, A novel peptide hydrogel for an antimicrobial bandage contact lens, *Adv. Healthcare Mater.*, 2016, **5**(16), 2013–2018.

31 A. G. Gallagher, *et al.*, Development of a Poly-ε-Lysine Contact Lens as a Drug Delivery Device for the Treatment of Fungal Keratitis, *Invest. Ophthalmol. Visual Sci.*, 2017, **58**(11), 4499–4505.
32 S. Kennedy, *et al.*, Poly-ε-lysine based hydrogels as synthetic substrates for the expansion of corneal endothelial cells for transplantation, *J. Mater. Sci.: Mater. Med.*, 2019, **30**(9), 102.
33 B. Kadler, A 3D in vitro co-culture to model peripheral nerve myelination using functionalised poly(ε -lysine) scaffolds, in *Faculty of Medical and Human Sciences*, The University of Manchester, 2015, p. 119.
34 S. S. Negah, *et al.*, Laminin-derived Ile-Lys-Val-ala-Val: a promising bioactive peptide in neural tissue engineering in traumatic brain injury, *Cell Tissue Res.*, 2018, **371**(2), 223–236.
35 R. Patel, *et al.*, Ile-Lys-Val-ala-Val (IKVAV) peptide for neuronal tissue engineering, *Polym. Adv. Technol.*, 2019, **30**(1), 4–12.
36 H. Hosseinkhani, *et al.*, Engineering three-dimensional collagen-IKVAV matrix to mimic neural microenvironment, *ACS Chem. Neurosci.*, 2013, **4**(8), 1229–1235.
37 A. Sorensen, *et al.*, Astrocytes, but not olfactory ensheathing cells or Schwann cells, promote myelination of CNS axons in vitro, *Glia*, 2008, **56**(7), 750–763.
38 M. V. Sofroniew and H. V. Vinters, Astrocytes: biology and pathology, *Acta Neuropathol.*, 2010, **119**(1), 7–35.
39 P. O'Neill, *et al.*, Sulfatase-mediated manipulation of the astrocyte-Schwann cell interface, *Glia*, 2017, **65**(1), 19–33.
40 H. Kıray, *et al.*, The multifaceted role of astrocytes in regulating myelination, *Exp. Neurol.*, 2016, **283**, 541–549.
41 P. S. Donoghue, *et al.*, The development of a ε-polycaprolactone scaffold for central nervous system repair, *Tissue Eng., Part A*, 2012, **19**(3–4), 497–507.
42 A. Sørensen, *et al.*, Long-term neurite orientation on astrocyte monolayers aligned by microtopography, *Biomaterials*, 2007, **28**(36), 5498–5508.
43 A. Varone, *et al.*, The potential of Antheraea pernyi silk for spinal cord repair, *Sci. Rep.*, 2017, **7**(1), 13790.
44 J. M. Zuidema, R. J. Gilbert and M. K. Gottipati, Biomaterial Approaches to Modulate Reactive Astroglial Response, *Cells Tissues Organs*, 2018, **205**(5–6), 372–395.
45 J. Schiweck, B. J. Eickholt and K. Murk, Important shapeshifter: mechanisms allowing astrocytes to respond to the changing nervous system during development, injury and disease, *Front. Cell. Neurosci.*, 2018, **12**, DOI: 10.3389/fncel.2018.00261.
46 J. P. Frampton, *et al.*, Fabrication and optimization of alginate hydrogel constructs for use in 3D neural cell culture, *Biomed. Mater.*, 2011, **6**(1), 015002.
47 S. Balasubramanian, *et al.*, Three-dimensional environment sustains morphological heterogeneity and promotes phenotypic progression during astrocyte development, *Tissue Eng., Part A*, 2016, **22**(11–12), 885–898.
48 A. L. Placone, *et al.*, Human astrocytes develop physiological morphology and remain quiescent in a novel 3D matrix, *Biomaterials*, 2015, **42**, 134–143.
49 T. B. Puschmann, *et al.*, Bioactive 3D cell culture system minimizes cellular stress and maintains the in vivo-like morphological complexity of astroglial cells, *Glia*, 2013, **61**(3), 432–440.
50 W.-W. Hu, *et al.*, Morphology and functions of astrocytes cultured on water-repellent fractal tripalmitin surfaces, *Biomaterials*, 2014, **35**(26), 7386–7397.
51 P. C. Georges, *et al.*, Matrices with compliance comparable to that of brain tissue select neuronal over glial growth in mixed cortical cultures, *Biophys. J.*, 2006, **90**(8), 3012–3018.
52 C. A. McKay, *et al.*, An injectable, calcium responsive composite hydrogel for the treatment of acute spinal cord injury, *ACS Appl. Mater. Interfaces*, 2014, **6**(3), 1424–1438.
53 C. C. Winter, *et al.*, Transplantable living scaffolds comprised of micro-tissue engineered aligned astrocyte networks to facilitate central nervous system regeneration, *Acta Biomater.*, 2016, **38**, 44–58.
54 C. L. Lau, *et al.*, 3D Electrospun scaffolds promote a cytotrophic phenotype of cultured primary astrocytes, *J. Neurochem.*, 2014, **130**(2), 215–226.
55 S. A. Liddelow and B. A. Barres, Reactive astrocytes: production, function, and therapeutic potential, *Immunity*, 2017, **46**(6), 957–967.
56 M. Morita, *et al.*, Dual regulation of calcium oscillation in astrocytes by growth factors and pro-inflammatory cytokines via the mitogen-activated protein kinase cascade, *J. Neurosci.*, 2003, **23**(34), 10944–10952.
57 A. C. Wolfes, *et al.*, A novel method for culturing stellate astrocytes reveals spatially distinct Ca2+ signaling and vesicle recycling in astrocytic processes, *J. Gen. Physiol.*, 2017, **149**(1), 149–170.
58 L. C. Foo, *et al.*, Development of a method for the purification and culture of rodent astrocytes, *Neuron*, 2011, **71**(5), 799–811.
59 L. F. Eng, *et al.*, An acidic protein isolated from fibrous astrocytes, *Brain Res.*, 1971, **28**(2), 351–354.
60 S. Hockfield and R. D. McKay, Identification of major cell classes in the developing mammalian nervous system, *J. Neurosci.*, 1985, **5**(12), 3310–3328.
61 U. Lendahl, L. B. Zimmerman and R. D. G. McKay, CNS stem cells express a new class of intermediate filament protein, *Cell*, 1990, **60**(4), 585–595.
62 S. R. Clarke, *et al.*, Reactive astrocytes express the embryonic intermediate neurofilament nestin, *NeuroReport*, 1994, **5**(15), 1885–1888.
63 R. C. S. Lin, *et al.*, Re-expression of the intermediate filament nestin in reactive astrocytes, *Neurobiol. Dis.*, 1995, **2**(2), 79–85.
64 A. Jagielska, *et al.*, Mechanical environment modulates biological properties of oligodendrocyte progenitor cells, *Stem Cells Dev.*, 2012, **21**(16), 2905–2914.
65 T. Liu, *et al.*, Nanofibrous collagen nerve conduits for spinal cord repair, *Tissue Eng., Part A*, 2012, **18**(9–10), 1057–1066.

66 F. Gelain, *et al.*, Transplantation of nanostructured composite scaffolds results in the regeneration of chronically injured spinal cords, *ACS Nano*, 2010, **5**(1), 227–236.
67 E. A. J. Joosten, P. R. Bär and W. H. Gispen, Collagen implants and cortico-spinal axonal growth after mid-thoracic spinal cord lesion in the adult rat, *J. Neurosci. Res.*, 1995, **41**(4), 481–490.
68 R. Marchand and S. Woerly, Transected spinal cords grafted with in situ self-assembled collagen matrices, *Neuroscience*, 1990, **36**(1), 45–60.
69 S. Woerly, *et al.*, Prevention of gliotic scar formation by NeuroGel™ allows partial endogenous repair of transected cat spinal cord, *J. Neurosci. Res.*, 2004, **75**(2), 262–272.